

~~Metall. Trans~~

Submitted to Metall. Trans

3/23/99

(Accepted)

REACTIVE INFILTRATION OF SILICON MELT THROUGH MICROPOROUS AMORPHOUS CARBON PREFORMS

P. Sangsuwan¹, S.N. Tewari², J.E. Gatica³, M. Singh⁴, and R. Dickerson⁴

Department of Chemical Engineering,
Cleveland State University, Cleveland, OH 44115-2425

ABSTRACT

d

have The kinetics of unidirectional capillary infiltration of silicon melt into microporous carbon preforms has been investigated as a function of the pore morphology and melt temperature. The infiltrated specimens showed alternating bands of dark and bright regions, which corresponded to the unreacted free carbon and free silicon regions, respectively. The decrease in the infiltration front velocity for increasing infiltration distances, is in qualitative agreement with the closed-form solution of capillarity driven fluid flow through constant cross section cylindrical pores. However, drastic changes in the thermal response and infiltration front morphologies were observed for minute differences in the preforms microstructure. This suggests the need for a dynamic percolation model that would account for the exothermic nature of the silicon-carbon chemical reaction and the associated pore closing phenomenon.

I. INTRODUCTION

Exothermic reactions between a porous matrix and infiltrating melt provide a more economic alternative for synthesizing many ceramics, intermetallics and composites. In reaction bonded silicon carbide, capillary infiltration of carbon containing body, usually also containing a large amount of SiC grains as inert fillers, is carried out by molten silicon^[1]. The exothermic reaction between silicon and carbon results in the formation of silicon carbide particles that bond the previously existing SiC grains. In another approach, carbonaceous materials, such as, carbon fiber tow, carbon fiber cloth or felt, are infiltrated by molten silicon in vacuum to form Si/SiC (silicon carbide reinforced silicon composites)^[1]. It has recently been demonstrated that infiltration of cast microporous carbon preforms by silicon melt can be used to fabricate high

¹ Graduate Student

² Professor

³ Associate Professor, author to whom all correspondence must be addressed

⁴ Senior Research Engineer, NYMA, Inc., Lewis Research Center Group, Cleveland, OH 44135

density, near net shaped, silicon carbide components at significantly reduced cost^[2,3]. Components, fabricated by this technique, are expected to find applications as gas turbine engine components or commercial combustion nozzles, where their refractoriness (high elevated temperature strength), good oxidation resistance, high thermal conductivity, low density and adequate toughness can be fully exploited. However, successful commercial exploitation of this technique requires a quantitative understanding of the various steps involved in the process.

The siliconization mechanism has been extensively studied via experiments on isolated carbon fibers or plates^[4-9]. Since molten silicon wets carbon, it wicks up into the microporous carbon preform when it is brought in contact with the preform, thus converting carbon into silicon carbide. It was initially believed that after a thin film of silicon carbide forms on the carbon surface, diffusion of silicon or carbon through the solid SiC (the melting point of silicon carbide, 2100 K, is much higher than that of silicon, 1687 K) is responsible for further conversion^[4,5]. Grain boundary diffusion was initially invoked to explain the fast conversion kinetics that is generally observed. It was later proposed that the initial silicon carbide layer spalls off due to the volume increase caused by the reaction, exposing a fresh carbon surface to liquid silicon, with further conversion occurring by dissolution of carbon into molten silicon at higher temperatures, followed by the precipitation of silicon carbide in regions of lower temperatures^[6-8].

However, there has been very little effort to study the most important step in the conversion process: the process of silicon infiltration through the porous carbon preforms. Unlike in other infiltration processes where there is no reaction between the porous preforms and the infiltrating liquid, here, the reaction between the infiltrating silicon melt and carbon results in a reduced pore size (there is an approximate 58% volume increase for each mole of silicon carbide formed). This reduces the permeability of the preform and decreases the infiltration velocity. Therefore, if the initial pore size of the preform is small, the silicon infiltration can prematurely stop, resulting in an incomplete infiltration, frequently referred to as "choking". Alternatively, if channel sizes are too large, the preform would be fully infiltrated, but unreacted silicon may remain in the component. Messner and Chiang^[9] formulated an analytical model based on Darcy's law^[10]. This model contained an approximate varying preform permeability law, and it was used to predict the infiltration behavior of silicon through graphite preforms. However,

no measurement of the infiltration kinetics was carried out. There is only one study reported in the literature^[11], where an attempt has been made to measure the infiltration front velocity as a function of temperature. Einset^[11] exposed thin carbon tapes, fabricated by two different techniques, to silicon melt in order to examine the infiltration kinetics. Thermocouples were inserted at different lengths along the tapes to monitor the propagation of the infiltrating reaction front. These experiments, however, do not accurately represent infiltration through the porous preform because silicon melt would preferentially *wet and traverse along the outer surface* of the preforms (tapes) where there is no resistance to the melt flow, and not through the interior tortuous channels.

The purpose of this research was to examine the interplay between chemical kinetics and capillary flow for silicon infiltration into microporous carbon preforms. The investigation focussed on the effect of pore structure and processing conditions on the infiltration process. Two types of carbon preforms were infiltrated at four different melt temperatures (1703, 1743, 1788, and 1853 K). The infiltration dynamics ~~was~~ *were* measured with the help of thermocouples imbedded in the preforms.

II. EXPERIMENTAL PROCEDURE

II.1. MICROPOROUS CARBON PREFORMS

The microporous amorphous carbon preforms used in this study were made from a mixture of furfuryl alcohol resin, diethylene and triethylene glycols and p-toluene sulfonic acid. This mixture was polymerized to form a porous solid polymer. The solid polymer was then heated slowly up to 970 K in a flowing argon atmosphere, which resulted in the production of microporous carbon preforms. Preforms with a range of pore sizes were obtained by varying the composition of the organic mixture. Further details of the preform fabrication can be found elsewhere^[3]. The microstructure of the preforms was examined by scanning electron microscopy, and characterized by mercury porosimetry and permeability determinations.

During mercury porosimetry, the porous preform is immersed into a mercury bath, and the

intruded volume of mercury is measured as a function of the applied hydrostatic pressure. This information is then used to obtain the incremental intrusion volume (per unit weight) of the porous specimen as a function of the equivalent diameter of cylindrical pores. The incremental intrusion area (per unit weight) as a function of the pore diameter is also obtained. These data are then used to obtain the pore size distributions, based either on the pore volumes or the pore areas. Knowing the bulk density and the total intruded volume the skeletal density is determined assuming that the pores are continuous, i.e., no isolated pores exist in the specimen.

Permeability determinations consisted of measuring water flow rates through the preforms as a function of the applied pressure gradient. Darcy's law^[10] was then used to correlate the measurements and obtain the preform permeabilities, $\langle \kappa \rangle$.

II.2. ANALYSIS OF SILICON MELT INFILTRATION

Figure 1 shows a schematic view of the experimental set up used to analyze the process of silicon melt infiltration through the porous preforms, as a function of the melt temperature. Four closed-end holes were drilled along the length of the cylindrical carbon preforms (1.27 cm in diameter and 4.6 cm in length) on one end. Tungsten-rhenium thermocouples, kept inside twin bored alumina sheaths, were then inserted into these holes, such that their tips would be located at 0.3, 0.5, 0.8 and 1.1 cm from the (bottom) end of the preform to be immersed into the silicon melt. The side surface of the preform was coated with a refractory paste to avoid side infiltration of silicon, and ensure unidirectional infiltration. The preform was then inserted in an alumina tube (#12) which was rigidly fixed to the top insulator (#2). An induction power supply (#4) was used to heat the graphite susceptor (#5). This, in turn, heated the preform, hanging from above, and the silicon melt contained in a quartz crucible (#8) kept below. A thermocouple (#1) recorded the temperature of the silicon melt. The whole assembly was kept under a vacuum-controlled atmosphere inside a transparent chamber. Silicon (99.9995% purity) was first melted in a flowing argon atmosphere, and then brought to the desired experiment temperature. The silicon melt containing crucible was then raised, bringing the melt level to about 0.5 cm away from the bottom surface of the carbon preform. Once the preform and the melt had reached thermal equilibrium, the crucible was rapidly raised to immerse about 1.5 cm of the preform into the

silicon melt, and initiate the silicon infiltration process. After approximately 2 minutes, the crucible was again lowered, and the induction power was switched off. The thermal responses of the thermocouples as a function of time, kept in the preform and in the silicon melt, were continuously recorded with the help of a Hewlett Packard data logger. After the infiltrated sample was cooled to room temperature, it was taken out, sectioned, and examined by optical and scanning electron metallography, and electron microprobe analysis.

III. RESULTS

III.1. MICROSTRUCTURAL CHARACTERIZATION OF THE PREFORMS

Figure 2 shows typical microstructures of the two types of microporous carbon preforms used in this study. The carbon struts are bridged with each other, and the inter-strut regions provide an interconnected continuous porosity. Type "B" preform appears to be more open, when compared with type "A". The three-dimensional network of interconnected pores does not appear to have any anisotropy.

Figure 3 presents the results of porosimetry determinations carried out on two different preforms. The percent intrusion volume (Figure 3a), the percent intrusion area (Figure 3b) versus the pore diameter, and the corresponding pore size distributions (Figures 3c and 3d). Both preforms show a narrow pore size distribution. Their median pore diameters, based either on the pore volume or on the pore surface area, are nearly identical (cf. Table 1). A comparison between their skeletal densities, 1.48 and 1.51 g cm⁻³, and the literature reported density of glassy carbon, 1.5 g cm⁻³, suggests that the pore networks in these preforms are interconnected. In the presence of isolated pores, the skeletal density calculated from mercury porosimetry would be smaller than that corresponding to glassy carbon. However, the "B" type preform is more porous when compared with the "A" type, as shown by their fraction porosities, 0.53 versus 0.48 (cf. Table 1). The pore surface area per unit pore volume corresponding to the type "A" preform is approximately 24% larger than that of preform of type "B". "A" having a smaller average pore diameter also indicates this, 0.10 versus 0.14 μm (with the average pore diameter found as $4V/A$, where, V is the total

intrusion volume, and A is the total intrusion surface area).

Table 1. Mercury porosimetry and permeability results for microporous carbon specimens.

Characteristics	Type A	Type B
Median pore diameter (μm)	1.42	1.25
Average pore diameter (μm)	1.56	1.49
Fraction porosity	0.48	0.53
Bulk density (g cm^{-3})	0.77	0.70
Skeletal density, (g cm^{-3})	1.48	1.51
Pore area per unit pore volume $\times 10^{-7}$, m^{-1}	3.64	2.93
Permeability $\times 10^{14}$ (m^2)	2.29 ± 0.03	2.70 ± 0.01

III.2. PERMEABILITY ANALYSIS OF UNINFILTRATED SPECIMENS

The porous medium permeability, κ , is an overall macroscopic parameter which is widely used to describe fluid flow through porous structures in many engineering applications. For a Boussinesq's fluid, Darcy's law^[10] is:

$$\rho_f^o \frac{\partial \bar{u}}{\partial t} = -\bar{\Delta} p - \frac{\mu_f}{\kappa} \bar{u} - \rho_f^o [\beta_T (T - T^o) + \beta_C (C - C^o)] \bar{g} \quad (1)$$

Assuming steady-state conditions and neglecting buoyancy effects, for unidirectional flow, Darcy's relationship reduces to,

$$v = -\frac{\kappa}{\mu_f} \frac{\partial p}{\partial z} \quad (2)$$

which, can be easily solved assuming a linear dependence for the pressure. This relationship can be used to extract the permeability of the medium, from a linear correlation between fluid flow velocity (v) and the applied pressure gradient. The goodness of fit of the determinations

corresponding to preforms of type "A" and "B" (cf. Figure 4), supports the applicability of the Darcy's law for the preforms used in this study. For a room temperature viscosity of water of 9.6×10^{-10} MPa s, the permeabilities of the two preforms, "A" and "B", can be easily estimated as shown in Table 1.

III.3. MICROSTRUCTURAL ANALYSIS OF INFILTRATED SPECIMENS

Figure 5 shows typical microstructures after infiltration. Figure 5a shows an overall view of a specimen after infiltration. The bottom 1.7-cm of this preform was dipped into the silicon melt. The white layer is the boron nitride coating, while the dark layer is the silicon stuck to the boron nitride coating. This dark layer and the boron nitride coating underneath came off easily from the reacted specimen. Some silicon, which remained attached to the bottom surface when the preform was withdrawn from the melt, is indicated by an arrow.

Figure 5b shows longitudinal (parallel to the silicon infiltration direction) cross-sections for type "A" specimens which were infiltrated at melt temperatures of 1743, 1783, and 1853 K. The dark regions on the top of micrograph correspond to the uninfiltrated portions of the preform. The infiltrated portions of the preform appear at the bottom of the micrographs. At 1743 K, the type "A" preform was infiltrated up to a distance of about 0.28 cm before "choking" was observed. Instabilities developing at the front were observed with increasing melt temperature. For example, at a melt temperature of 1783 K, the infiltration front is no longer planar, instead, fingers of infiltrated regions protrude ahead of the overall infiltration front. At the highest melt temperature examined in this study, 1853 K, there is hardly any region that would appear to indicate the presence of a stable planar liquid infiltration front. The microstructure consists of a "swirling" pattern of isolated infiltrated regions.

The infiltrated portion of the specimens usually consists of alternating bands of dark and light contrast regions, marked as "D" and "B" in Figure 5b. Higher magnification views from these two regions are shown in Figure 6. The dark regions, Figure 6a, consist of silicon carbide grains (gray contrast), free silicon (white contrast), and unreacted carbon (black contrast). The large amount of unreacted carbon is responsible for the dark appearance of these regions. The bright

regions, Figure 6b, contain mostly silicon carbide and free silicon, with very little unreacted carbon present.

Typically, two types of cracks were observed in the infiltrated specimens (cf. Figure 7). The thermal stresses, resulting from the exothermic nature of the chemical reaction, can produce cracks in portions of the preform which are yet to be infiltrated as well as in the portions which have already been infiltrated. The bright looking silicon filled cracks (Figure 7a) must have formed before the preform was infiltrated with silicon melt, while the dark looking cracks (Figure 7b) were generated subsequent to the infiltration and reaction.

Figure 8 shows the longitudinal section through the infiltrated "B" type of porous carbon preforms (melt temperature 1743 K). For the same melt temperatures, the infiltration distance is significantly larger for the type "B" material, cf. 0.92 cm in Figure 8 against 0.28 cm in Figure 5b. The bright and dark bands observed for the type "A" preforms, at 1743 and 1783 K (Figure 5b), were also observed for the type "B" preform. However, the finger like instability observed for the type "A" material was not observed in type "B" material in the temperature range examined in this study (1703 K to 1853 K).

III.4. THERMAL RESPONSES DURING INFILTRATION

Typical temperature-time plots recorded by the thermocouple assembly described above, are shown in Figures 9a to 10c. The thermal response of the thermocouples located at 0.3, 0.5, 0.8 and 1.1 cm from the (bottom) surface of the preforms exposed to the silicon melt, are indicated as, TC1, TC2, TC3 and TC4, respectively. The thermal response corresponding to the silicon melt is indicated as Si.

III.4.a. Type "A" Preform

Figure 9a shows the thermal profiles obtained from infiltration experiments carried out with type "A" preforms. The uncertainty in the temperature values is approximately ± 6 K. The arrows in the figure bottom indicate the different stages of the infiltration experiments. The melt crucible was initially raised at 180 s. From 245 to 1655 seconds, the crucible was held stationary for the final

adjustment of the power supply to yield the desired melt temperature (1788 K), and until thermal equilibrium among the melt, the preform, and the surrounding susceptor is reached. The crucible was then raised at 1835 s, with the melt-carbon preform contact occurring at 1895 s, further crucible raising resulted in 1.7 cm of the preform being submerged into the melt. The exothermic reaction between the infiltrating silicon melt and the carbon preform resulted in a steep temperature rise, recorded by all thermocouples. It is worth noticing, however, that despite the highly exothermic reaction, the temperatures recorded by all preform thermocouples are back to the silicon melt temperature within 60 s after the initial temperature rise. After about two minutes of melt-preform contact, the crucible was pulled down (2015 s). The preform was out of the melt at about 2090 s, at which time the induction power was switched off. This resulted in a rapid cooling, approximately 50 K min^{-1} , recorded by all the five thermocouples. The isothermal plateau, starting at 2240 s, registered by the thermocouple in the silicon melt corresponds to the solidification of silicon (1687 K). It is interesting to note that the isothermal trend was also indicated by the thermocouples located in the preform, especially TC1, TC2, and to some extent TC3 (Figure 9c). This indicates the presence of free silicon in the preform, as it was previously suggested by the microstructural analysis (cf. Figure 6b). It also suggests that the silicon infiltration front reached a depth between TC3 and TC4, i.e. an infiltration distance between 0.5 and 0.8 cm. This is in agreement with the metallographically determined infiltration distance, 0.83 cm.

Figure 9b shows the thermal profiles in the vicinity of the temperature peaks. The rate of initial steep temperature rise decreases in the following order: 120 K s^{-1} for TC1 (located 0.3 cm from the silicon-carbon contact surface), 60 K s^{-1} for TC2 (0.5 cm), 55 K s^{-1} for TC3 (0.8 cm), and 25 K s^{-1} for TC4 (1.1 cm). It is interesting to note that the peak temperatures show a decrease with the increasing distance from the exposed surface of the preform. This is due to the continuous decrease in the infiltration front velocity as it travels into the preform, as predicted by the capillary flow analysis. Such thermal profiles can be used to estimate the infiltration front velocity for a quantitative comparison with theoretical predictions. The peak temperatures registered by the thermocouples, 2349 K (TC1), 2052 K (TC2), 1940 K (TC3) and 1859 K (TC4), also show a decreasing trend with the distance from the bottom surface.

III.4.b. Type "B" Preform

The thermal profiles obtained during the infiltration of type "B" preforms for the same conditions used for type "A" preforms (i.e., melt temperature 1788 K) are shown in Figures 10a-10c. The thermal responses of the four thermocouples imbedded in the preform indicate that the initial temperature rise rates, the peak temperatures, the energy evolved during the chemical reaction, and the time for the isothermal hold during the subsequent cooling, are all significantly larger than those corresponding to the experiments with type "A" preforms (cf. Figures 9a-9c). For example, the rates of initial temperature rise for the TC1 through TC4 thermocouples in the "B" preform are, 130, 175, 180, and 50 K s⁻¹ (cf. Figure 10a), as compared with 120, 60, 55, and 25 K s⁻¹ for type "A" (cf. Figure 9a), respectively. The maximum temperatures registered by the four thermocouples are, 2429, 2408, 2299, and 2245 K for type "B" (Figure 10b), as compared with 2349, 2052, 1940, and 1859 K for type "A" (cf. Figure 9b). The larger extent of infiltration of the "B" type of preform is also indicated by the considerably longer isothermal hold during cooling of the preform after the induction power is switched off, i.e. 90 s (B) vs. 55 s (A) (cf. Figures 10c and 9c). The thermal environment for the type "A" and "B" preforms appears to be the same as evidenced by the similar cooling rates, approximately 50 K min⁻¹, experienced after the induction power is switched off (cf. Figures 9c and 10c).

III.4.c. Typical Thermal Profiles in the Presence of Side Infiltration

Figure 11 shows the typical thermal profiles obtained in the presence of side infiltration due to the failure of boron nitride coating. The temperature scale, here, is indicated in mV because of the presence of thermal signals that are beyond the calibration limit of the thermocouple material. The propagating reaction pattern corresponding to unidirectional infiltration of the silicon melt (cf. Figures 9 and 10) is no longer observed. Instead, the thermal responses resemble more a chaotic propagation pattern. Here, the melt infiltrates from the side and from the bottom, causing an almost complete infiltration of the preform and its conversion into silicon carbide. This was experimentally observed.

IV. DISCUSSION

The analysis of capillarity-driven flow in a single pore can be used to describe flow through a porous medium, instead of using an overall characterization parameter (the medium permeability κ). For a single pore, the equations can be easily formulated based on Newton's law. For "highly" viscous fluids and for "short" infiltration lengths (neglecting end-effects and body forces) a closed-end form solution can be easily derived^[12],

$$z^2 = 2 \left[\frac{D_p^2 \rho_f}{16 \mu_f} \right]^2 \left[1 - \exp \left(- \frac{32 \mu_f}{D_p^2 \rho_f} t \right) \right] + \left[\frac{D_p^2 \rho_f}{16 \mu_f} \right] \left[\frac{4 \gamma_{LV} \cos(\theta)}{D_p \rho_f} - g z \right] t \quad (3)$$

which for short times, $t \ll D_p^2 \rho_f / 32 \mu_f$, becomes:

$$z^2 = \frac{D_p^2 \rho_f}{16 \mu_f} \left(\frac{4 \gamma_{LV} \cos(\theta)}{D_p \rho_f} - g z \right) t \quad (4)$$

For most cases where the flow occurs due to capillary pressure, the fluid weight is negligible at the early stages of the infiltration (i.e., for short infiltration lengths), when compared to the surface tension term, and the above equation becomes:

$$z^2 = \Phi t \quad \text{or, } v = \frac{\Phi}{2} \frac{1}{z} \quad (5)$$

with $\Phi = \frac{D_p \gamma_{LV} \cos \theta}{4 \mu_f}$

The parameter Φ , often termed as "intrinsic infiltration rate"^[13], can be obtained from the experimental data by plotting infiltration length or infiltration velocity versus infiltration time. One should notice, however, that the above equation has been derived for flow through a single pore, and is strictly valid for a porous structure of parallel pores of diameter " D_p ." Whereas, the experimental data will yield an overall Φ which is representative of the pore network (pore size, shape, distribution, and microstructure) being infiltrated. The " D_p " in the equation for Φ should therefore represent an "effective pore radius."

Let us examine the experimentally determined infiltration front velocity and its dependence on the infiltration length. Figures 12a and 12b show data for two infiltration experiments on type "B" preforms with a 1788 K silicon melt temperature. As anticipated by the capillary-flow analysis, the infiltration velocity decreased with the increasing infiltration distance (cf. Figure 12a). Least-squares analysis of the data in Figure 12b yield an approximate slope of $2 \times 10^{-5} \text{ m}^2 \text{ s}^{-1}$. One could assume the pore diameter, D_p , to be equal to the volume based median pore diameter, $1.25 \mu\text{m}$ (cf. Table 1), the liquid-vapor surface energy for silicon melt, γ_{LV} , to be $0.72\text{-}0.76 \text{ N m}^{-1}$ [5], the wetting angle (for C in vacuum), θ , to be between $0\text{-}22^\circ$ [15], and the viscosity of silicon, μ_f , to range between $0.46\text{-}0.76 \times 10^{-3} \text{ Pa s}$ [15]; then, according to Eq. (5), the intrinsic infiltration rate, Φ , will be $2.7\text{-}5.1 \times 10^{-4} \text{ m}^2 \text{ s}^{-1}$. This, for a preform porosity of 0.53 (cf. Table 1), will correspond to a theoretical slope ranging between $7.3\text{-}13.5 \times 10^{-5} \text{ m}^2 \text{ s}^{-1}$. Considering that the above analysis dealt with a single pore representation of a structure consisting of a randomly oriented array of multi-size pores, with the pores being assumed to remain unaltered during the infiltration process, the difference between the two (estimated and experimental) slope values is not surprising. It would appear as if the presence of a chemical reaction has an accelerating effect on the infiltration process, which is consistent with the evidence of free silicon observed for both types of preforms.

It is important to remember that any meaningful model of silicon infiltration through microporous carbon must account for the exothermic nature of the chemical reaction, and the accompanying changes in the pore morphology as a result of the chemical reaction. As it was mentioned before, the chemical reaction between the infiltrating silicon melt and carbon causes reduction in the pore size, while the temperature changes will alter physical properties and accelerate the chemical reaction. This would affect the melt flow through the pores, resulting in a different correlation between the infiltration front velocity and the infiltration distance. The two phenomena would then become intimately related as the chemical reaction, heat evolved, pore morphology, and capillary flow will interact with each other. For instance, Figure 13 shows the maximum temperature recorded by the thermocouples inserted in the preforms plotted against the thermocouple location (infiltration distance). The peak temperatures decrease for both the preforms, with the steepest decrease corresponding to the experiments in type "A" preforms. This indicates a higher propensity to pore closing for type "A" preforms. This was also observed

from the metallographic examination of the infiltrated "A" and "B" specimens. However, examination of their pore characteristics (Table 1) does not show any glaring differences between the two preforms. The only major differences are, the higher permeability of "B" (2.7 vs. $2.3 \times 10^{-14} \text{ m}^2$), and its smaller pore area per unit pore volume (2.93 vs. $3.64 \times 10^7 \text{ m}^{-1}$). One would, therefore, expect a larger extent of chemical reaction between carbon and silicon melt for the type "A" preform as compared with type "B" preforms, i.e. "A" would be more prone to exhibit pore closure. The capillarity-driven flow analysis, however, would predict similar behavior for both, type "A" and "B", preforms.

These observations indicate the need for a dynamic percolation model that would include the structural changes in the pores. The fluid contained within the micro-channels ($1\text{-}5 \mu\text{m}$) will interact thermally with the solid skeleton, and the local fluid properties would change drastically due to the very sharp temperature rise, up to $1000 \text{ }^\circ\text{C}$ (cf. Figures 9c and 10c). The species distribution will also be influenced. Since the structural changes are local phenomena, strongly influenced by the temperature and species distribution, any predictive tool must include, the dynamics of the flow environment, thermal interaction between the melt and solid, the temperature effects on the siliconizing process, and, the "after burning" of the free silicon, which is entrapped ahead of the "choking" front. In other words, a model based purely on flow analysis considerations, even when the pore structure were adapted dynamically to account for the occurrence of a chemical reaction, would not succeed in predicting the infiltration dynamics.

V. ACKNOWLEDGEMENTS

choking

Appreciation is expressed to Pat Dickerson, Dave Epperly, Jim Barker, and Christopher Palda for their technical assistance, and to Thomas K. Glasgow, Chief, Processing Science and Technology Branch, at the NASA-Lewis Research Center for partial support of this research.

VI. REFERENCES

- [1] Mehan, R.L. "Effect of Silicon Carbide Content and Orientation on the Properties of Si/SiC Ceramic Composite," *J. Amer. Ceram. Soc.*, 60(3-4), pp. 177-178 (1977).
- [2] Chiang, Y.M., R.P. Messner, C.D. Terwilliger and D.R. Behrendt, "Reaction Formed Silicon Carbide," *Mater. Sci. & Engng.*, A144, pp. 63-74 (1991).
- [3] Singh, M. and D.R. Behrendt, "Studies on the Reactive Melt Infiltration of Silicon and Silicon-Molybdenum Alloys in Porous Carbon", *NASA TM-105860* (1992).
- [4] Fitzer, E. and R. Gadow, "Investigation of the Reactivity of Different Carbons with Liquid Silicon," pp. 561-572 in *Proc. of International Symposium on Ceramics for Engines*, Japan (1983).
- [5] Minnear, W.P., "Interfacial Energies in the Si/SiC System and the Si+C Reaction," *Communications of the Amer. Cer. Soc.*, Jan. 1982, C-10-11.
- [6] Ness, J.N. and T.F. Page, "Microstructural Evolution in Reaction Bonded Silicon Carbide," *J. Mater. Sci.*, vol.21 (1986), 1372-1397.
- [7] Hase, T., H. Suzuki and T. Isekei, "Formation Process of β -SiC During Reaction Sintering," *J. Nuclear Materials*, vol. 59 (1976), 42-48.
- [8] Pampuch, P., E. Walasek and J. Bialoskorski, "Reaction Mechanism in Carbon-Liquid Silicon Systems at Elevated Temperatures," *Ceramics International*, vol 12 (1986), 99-106.

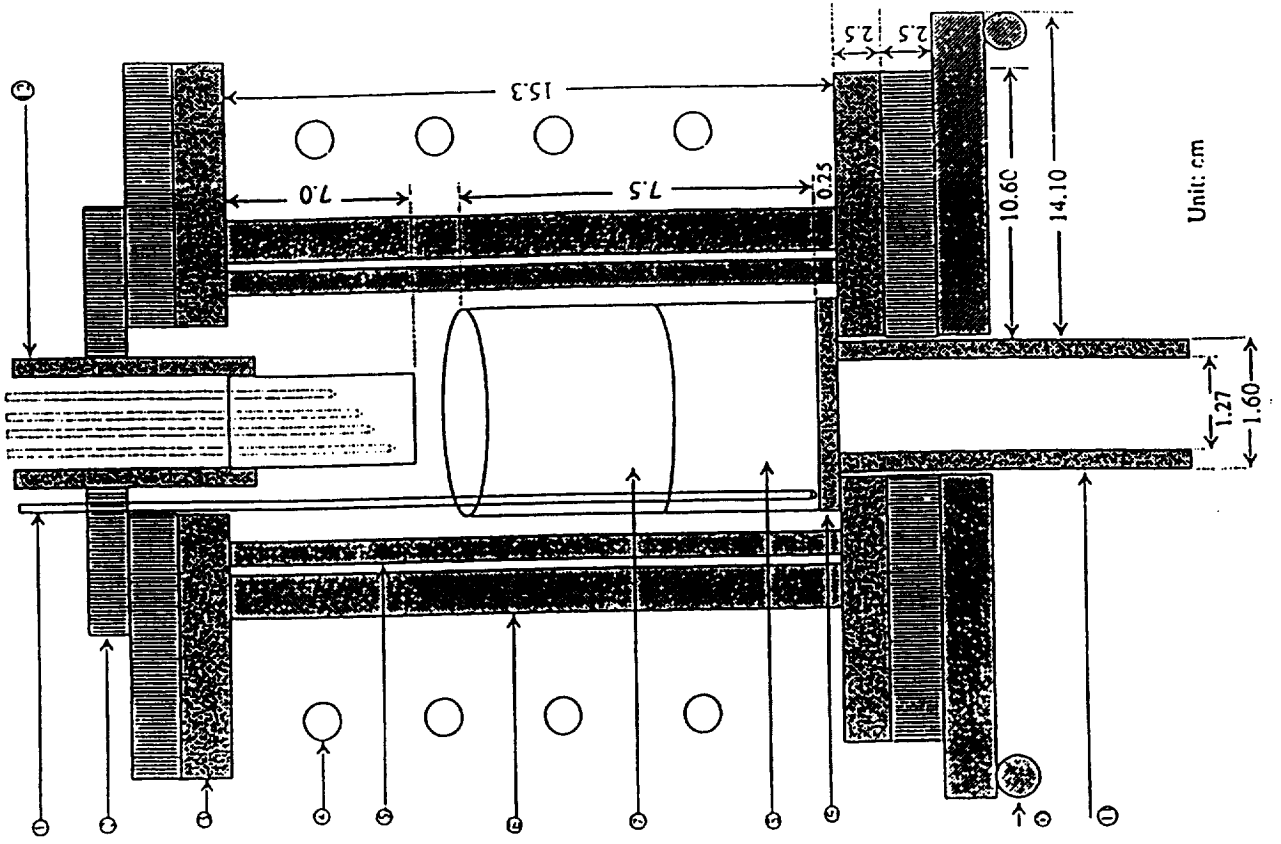
- [9] Messner, R.P. and Y.M. Chiang, "Liquid-Phase Reaction-Bonding of Silicon Carbide Using Alloyed Silicon-Molybdenum Melts," *J. Amer. Ceram. Soc.*, vol 73(5), (1990), 1193-1200.
- [10] Darcy, H.P.G., "Les fontaines publiques de la ville de Dijon, Exposition et application des principes a suivre et des formules a employer dans les questions de distribution d'eau," Victor Dalmont, Paris (1856).
- [11] Einset, E.O., "Capillary Infiltration Rates into Porous Media with Applications to Silcomp Processing," *J. Am. Ceram. Soc.*, 79(2), 333-338 (1996).
- [12] Martins, G.P., D.L. Olson and G.R. Edwards "Modeling of Infiltration Kinetics for Liquid Metal Processing of Composites," *Metall. Trans.*, 19B, pp. 95-101 (1988).
- [13] Hillig, W.B. "Making Ceramic Composites by Melt Infiltration," *Ceramic Bulletin*, 73(4), pp. 56-63 (1994).
- [14] Whalen, T.J. and A.T. Anderson, "Wetting of SiC, Si₃N₄, and Carbon by Si and Binary Si Alloys," *J. Amer. Ceram. Soc.*, vol. 58 [9-10], 1975, 396-399.
- [15] Turovskii, B.M. and I.I. Ivanova, "Temperature Dependence of the Viscosity of Fused Silicon," *Zvestiya Akademii Nauk SSSR, Neorganicheskie Materialy*, vol. 10 [12], December 1974, 2108-2111

LIST OF FIGURES

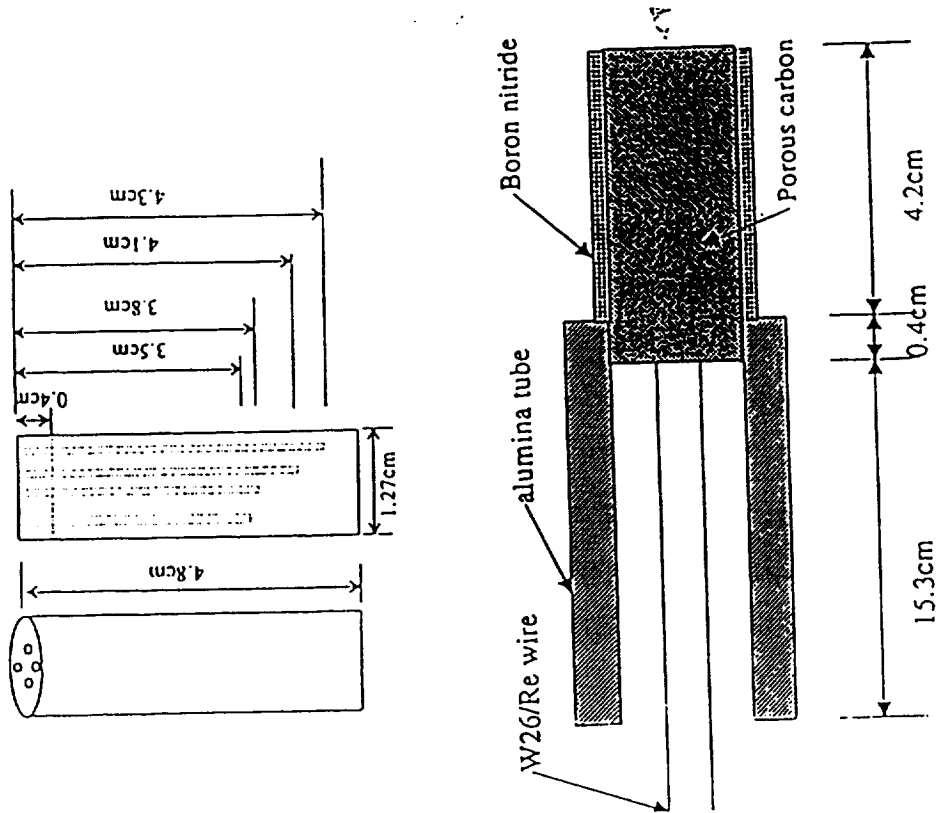
- Figure 1** Schematic view of the experimental apparatus for measuring silicon infiltration kinetics.
- Figure 2** Typical microstructure of porous amorphous carbon preform.
(a) Type "A", (b) Type "B".
- Figure 3** Typical pore characteristics of carbon preforms obtained by mercury porosimetry.
(a) Percent intrusion volume versus pore diameter.
(b) Percent intrusion area versus pore diameter.
(c) Percent incremental volume versus pore diameter.
(d) Percent incremental intrusion area versus pore diameter.
- Figure 4** Permeability determinations for type "A" and "B" microporous carbon preforms.
- Figure 5** Typical microstructure of the silicon infiltrated specimens.
(a) Typical overall view.
(b) Longitudinal (parallel to the infiltration direction) sections through the infiltrated "A" specimens. The dark contrast regions are marked "D", and light contrast regions are marked "B".
- Figure 6** Higher magnification views from the dark ("D") and light contrast ("B") regions of the infiltrated microstructure shown in Figure 5b.
- Figure 7** Typical cracks observed in the silicon melt infiltrated specimens.
(a) Cracks formed prior to infiltration.
(b) Cracks formed after infiltration and chemical reaction between carbon and silicon.

- Figure 8** Longitudinal (parallel to the infiltration direction) sections through the infiltrated "B" specimen (melt temperature 1743 K). The dark contrast regions are marked "D", and light contrast regions are marked "B".
- Figure 9** Thermal profiles recorded by the thermocouples located at 0.3, 0.5, 0.8 and 1.1 cm (TC1, TC2, TC3 and TC4, respectively) from the bottom surface of the type "A" preform, which was exposed to the silicon melt at 1788 K. Silicon melt profile is indicated by "Si".
- (a) Overall thermal profile.
 - (b) Thermal profiles in the vicinity of exothermic peaks.
 - (c) Thermal profile during cooling.
- Figure 10** Thermal profiles recorded by the thermocouples located at 0.3, 0.5, 0.8 and 1.1 cm (TC1, TC2, TC3 and TC4, respectively) from the bottom surface of the type "B" preform, which was exposed to the silicon melt at 1788 K. Silicon melt profile is indicated by "Si".
- (a) Overall thermal profile.
 - (b) Thermal profiles in the vicinity of exothermic peaks.
 - (c) Thermal profile during cooling.
- Figure 11** Thermal responses in the presence of side infiltration (Type "B" preform, infiltrated with Si melt at 1788 K).
- Figure 12** Decrease in the infiltration front velocity with increasing infiltration distance.
- Figure 13** The maximum (peak) temperatures recorded as a function of infiltration distance. The filled symbols are for "A" and open symbols are for "B" preforms.

SCHEMATIC OF EXPERIMENTAL ARRANGEMENT



Unit: cm



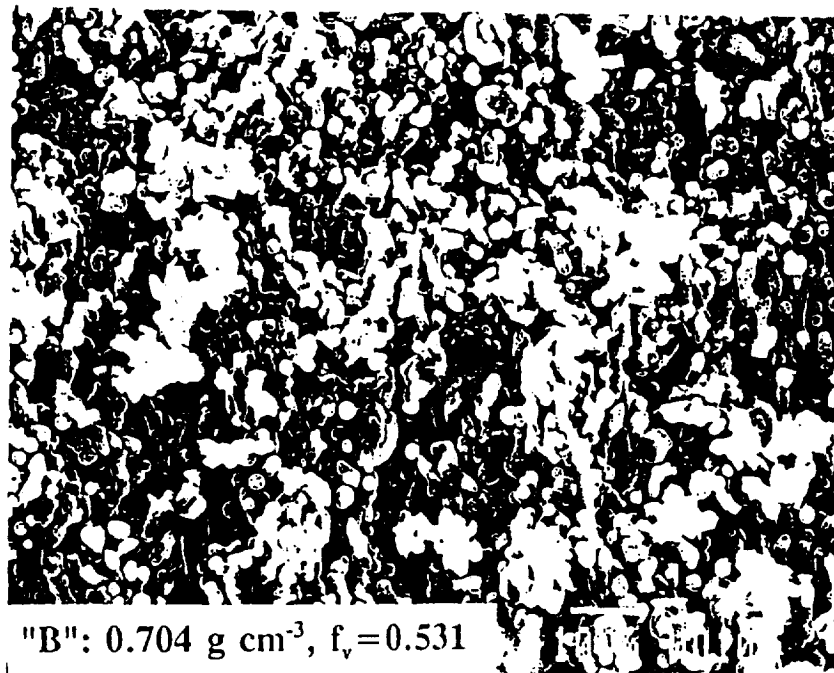
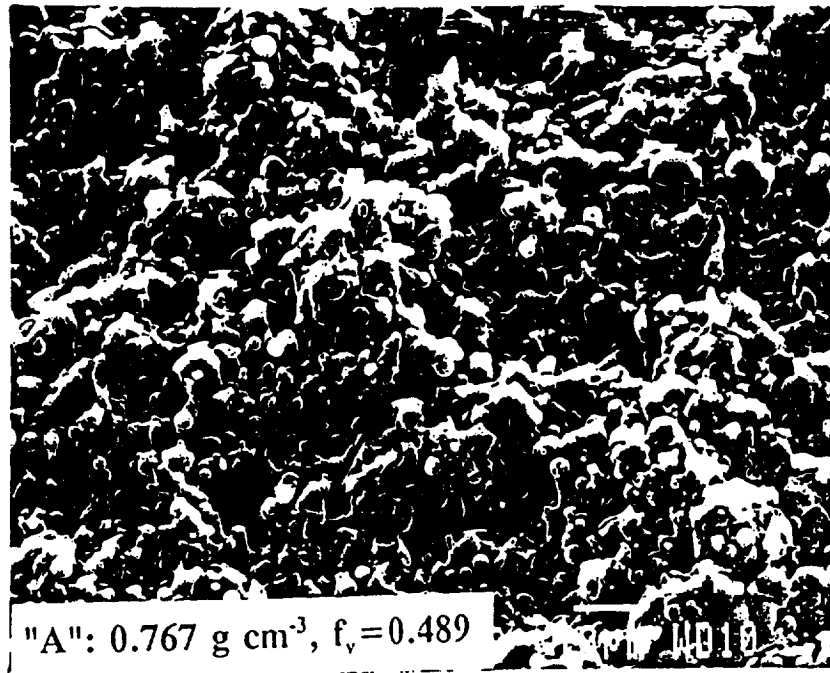


Fig. 2 Typical microstructure of porous carbon preform.
(a) Low magnification view of specimen type "A" and "B"

POROSIMETRY ANALYSIS OF MICROPOROUS CARBON PREFORMS

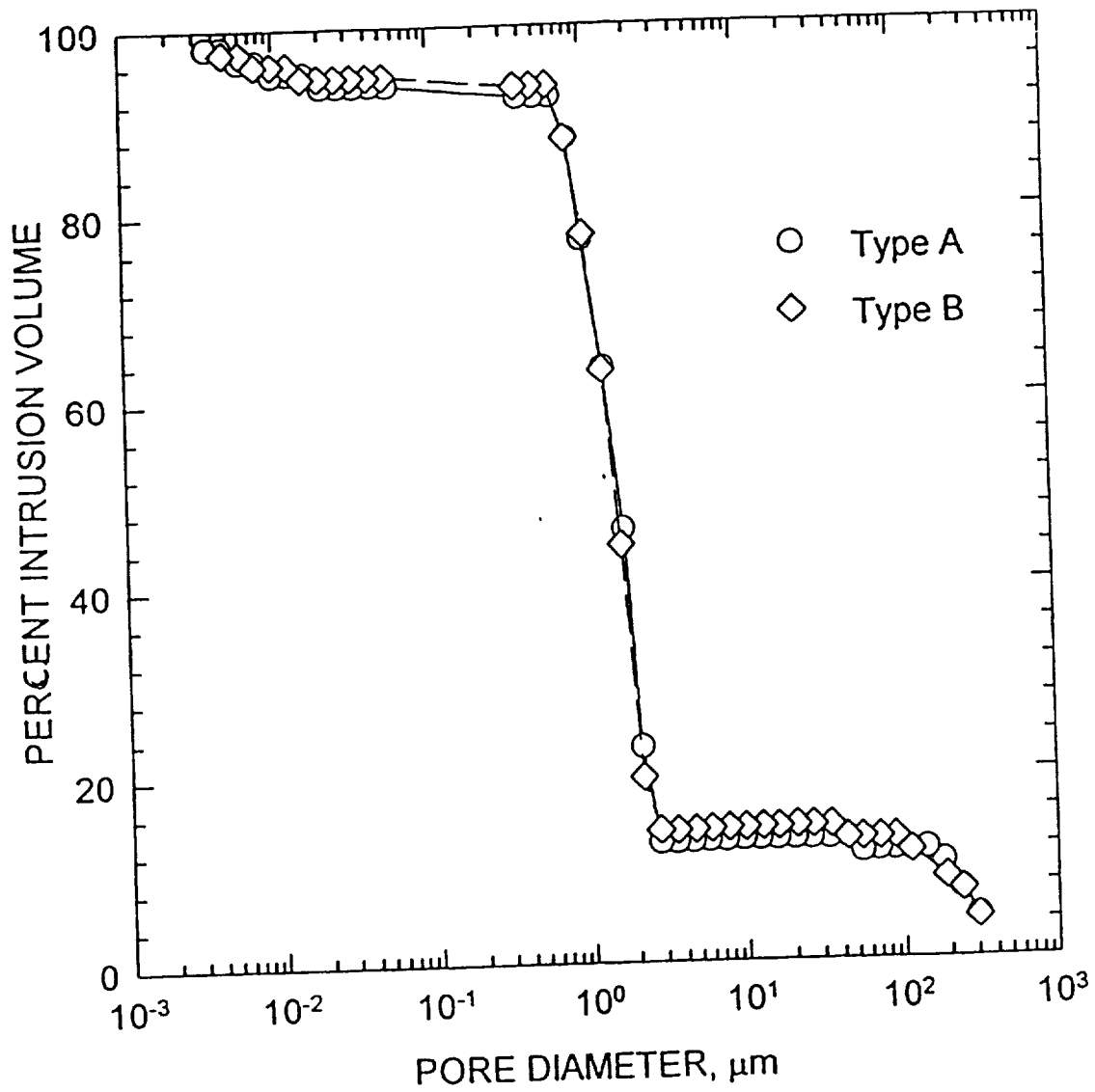


FIG 3 (a)

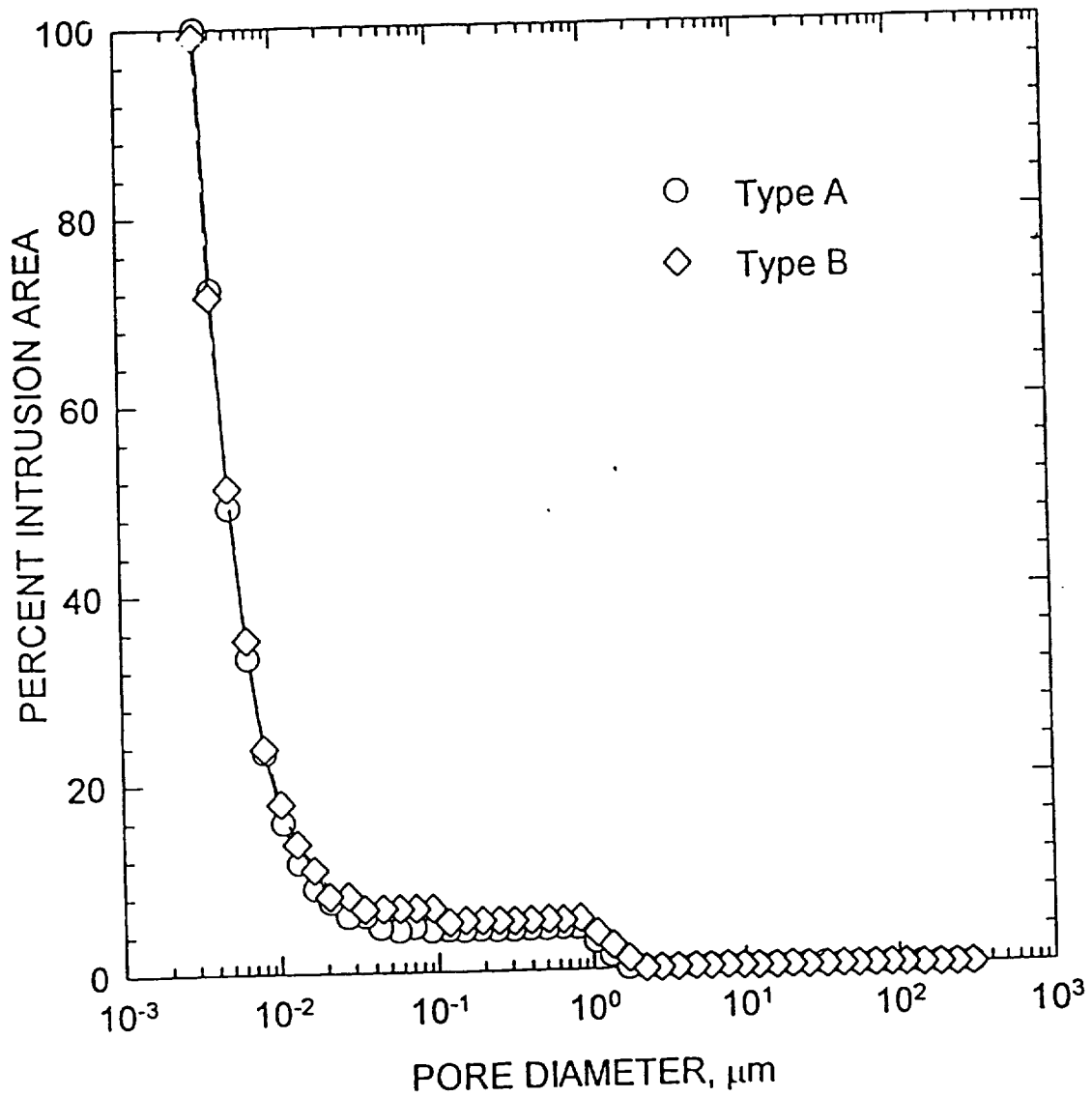


FIG 3 (b)

Porosimetry analysis of microporous carbon preforms

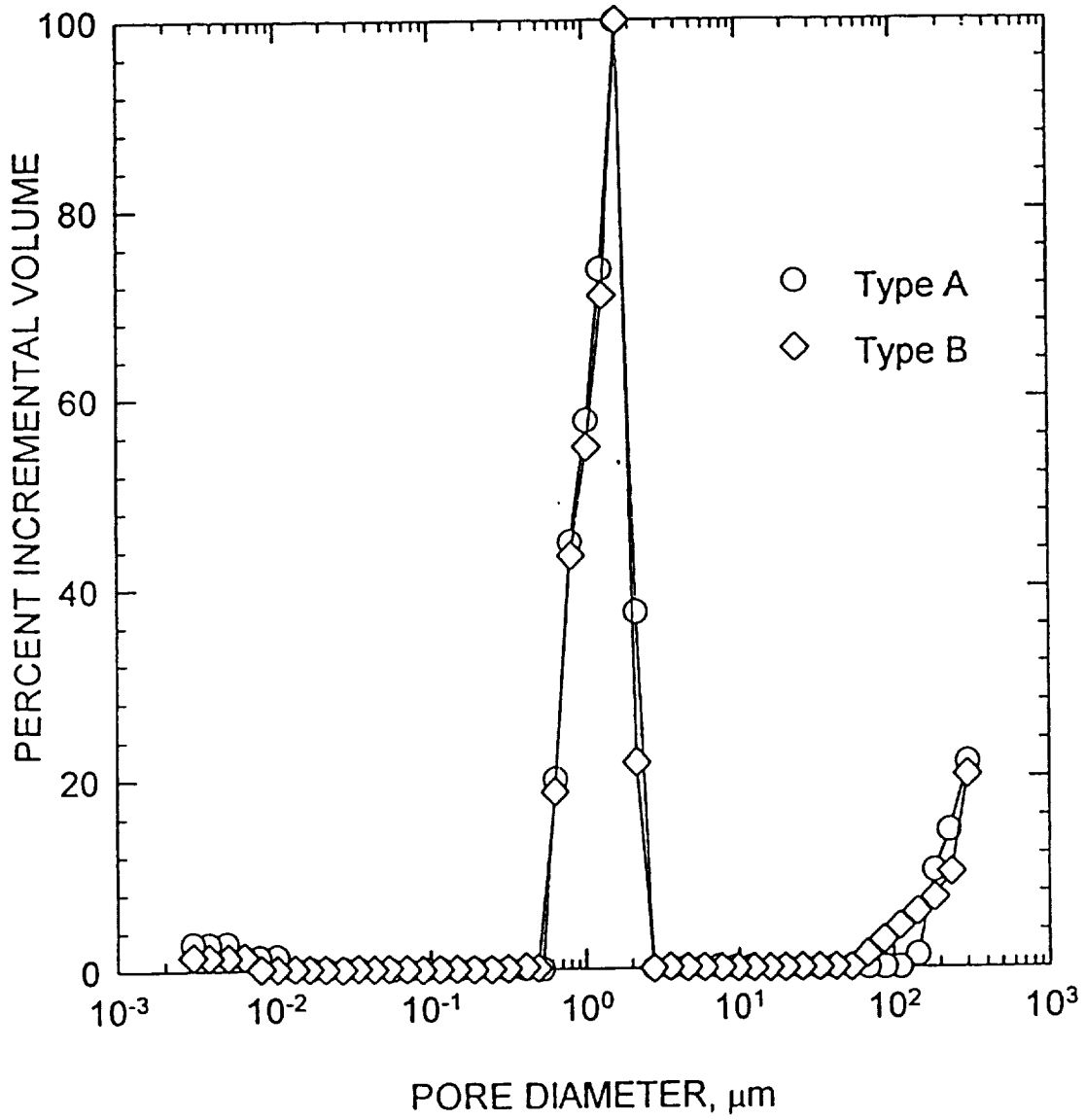


FIG. 3 (c)

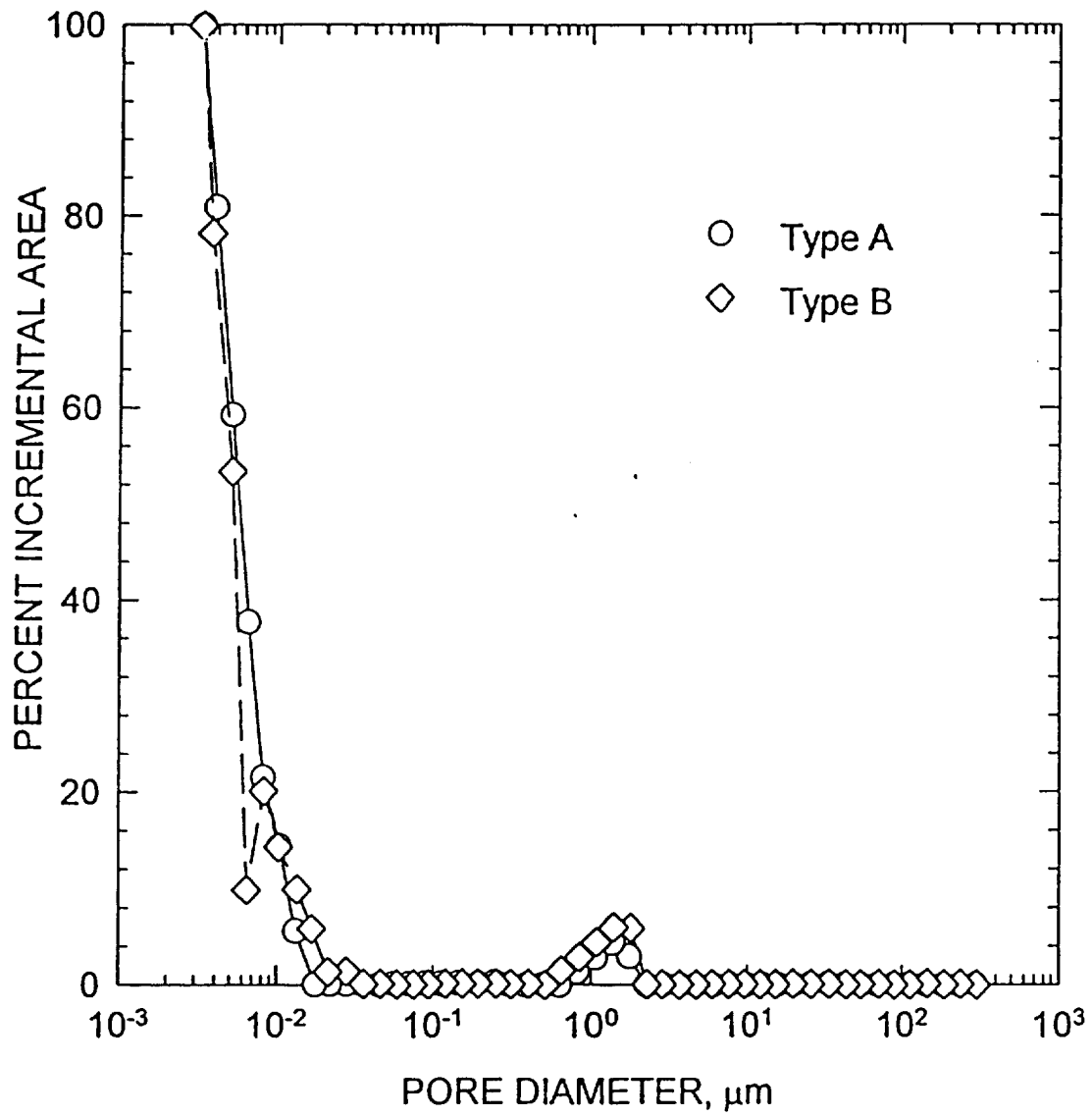


FIG. 3(a)

PERMEABILITY OF MICROPOROUS CARBON PREFORMS

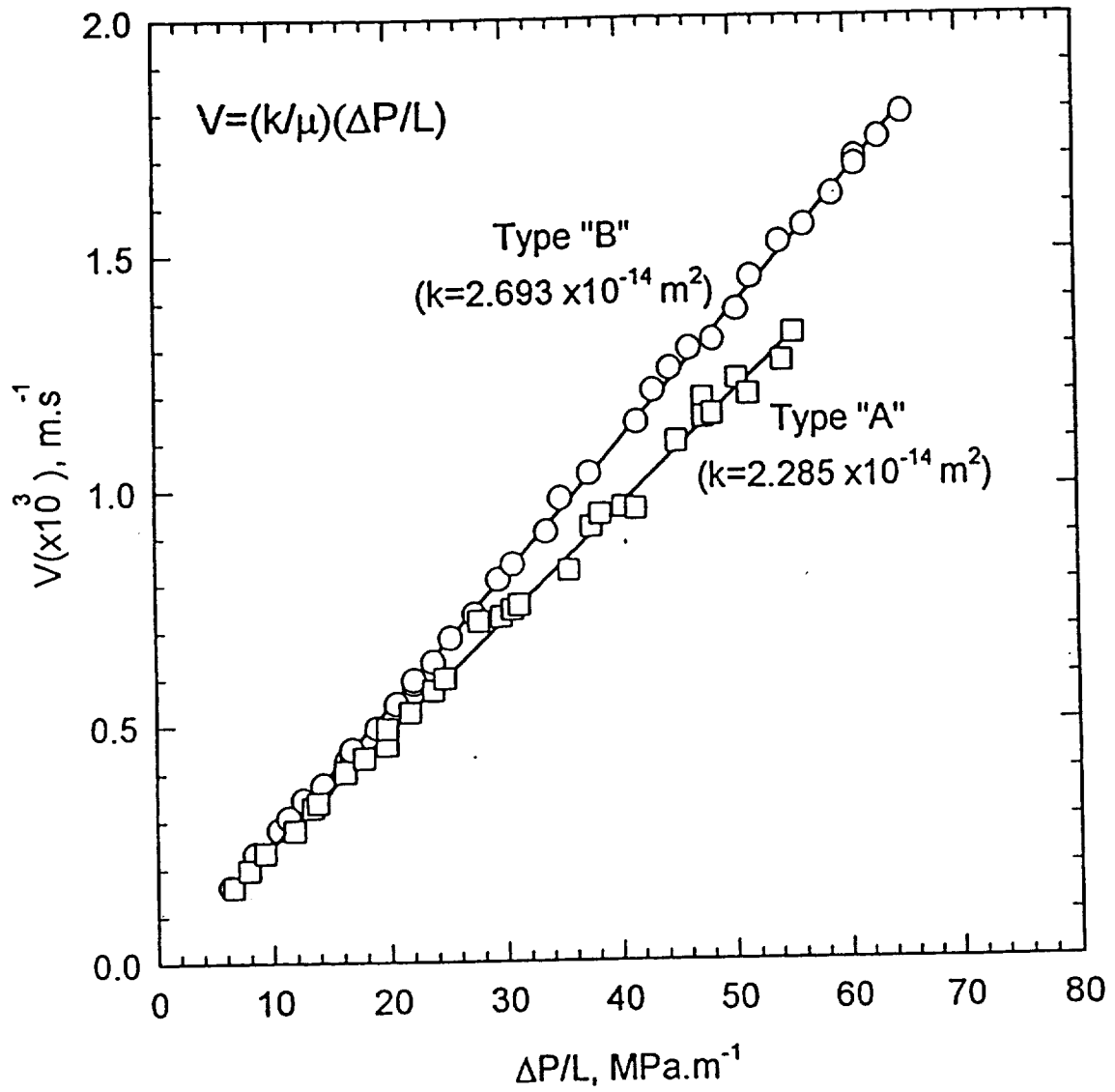


FIG. 4

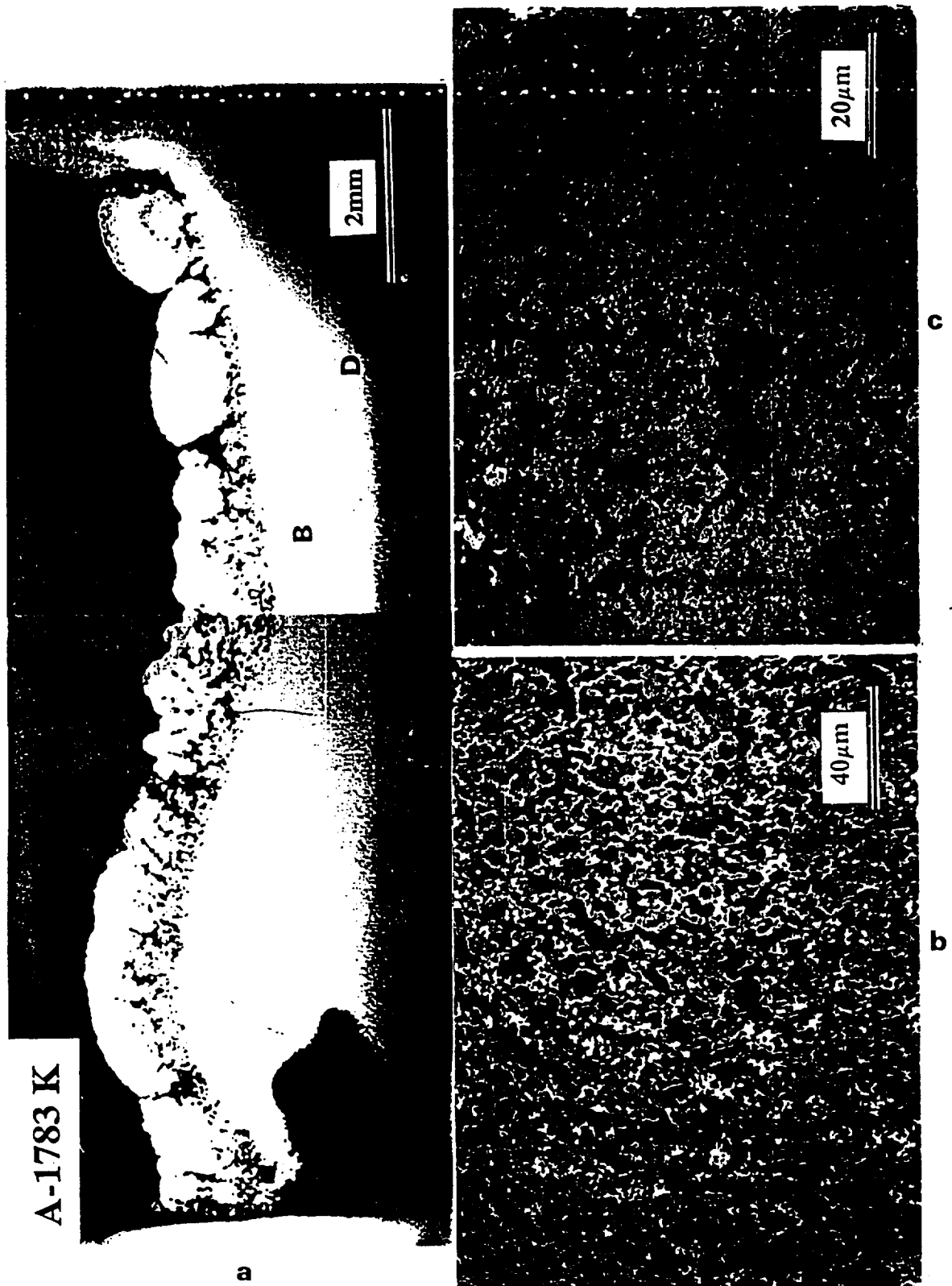
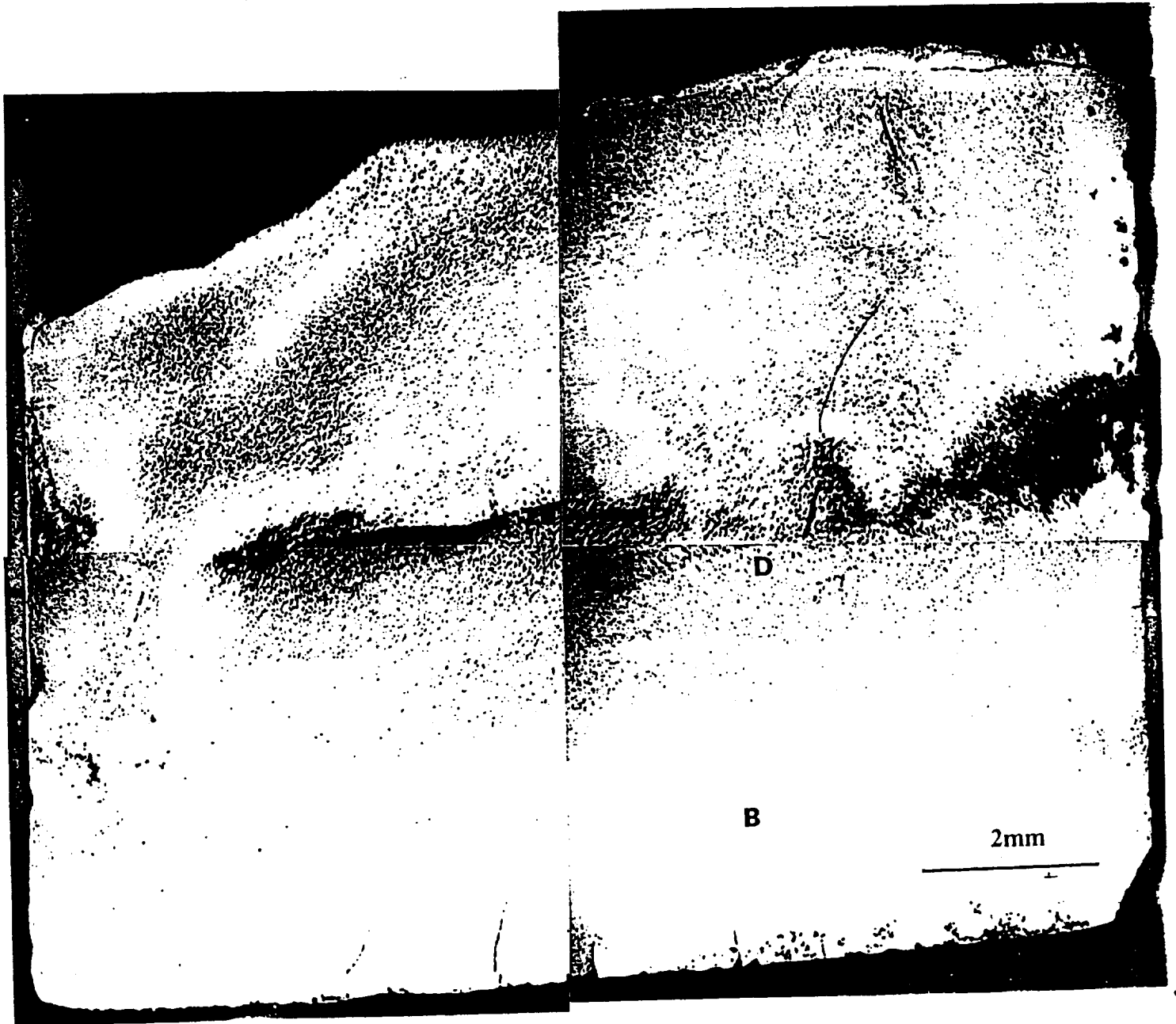
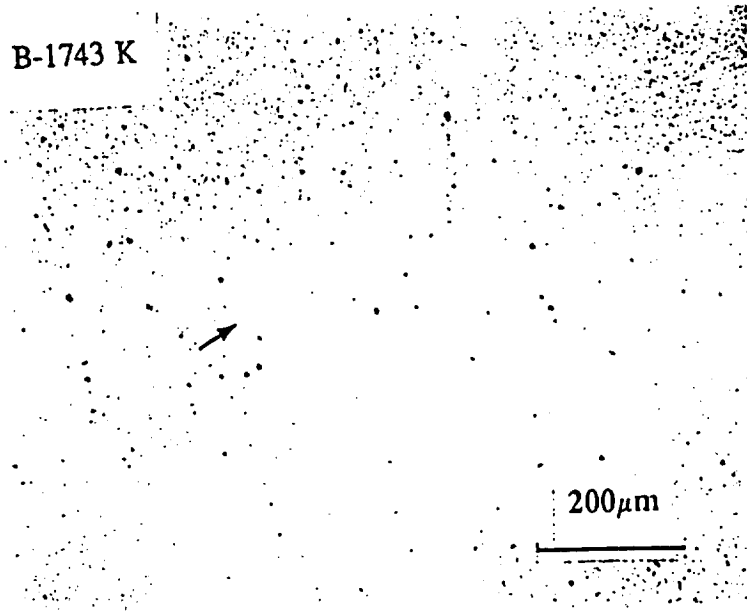


Fig. 5. Silicon infiltrated porous carbon type "A" 1783 K.
 (a) Longitudinal section (parallel to the silicon infiltration direction)
 (b) Region "D" high magnification
 (c) Region "B" high magnification

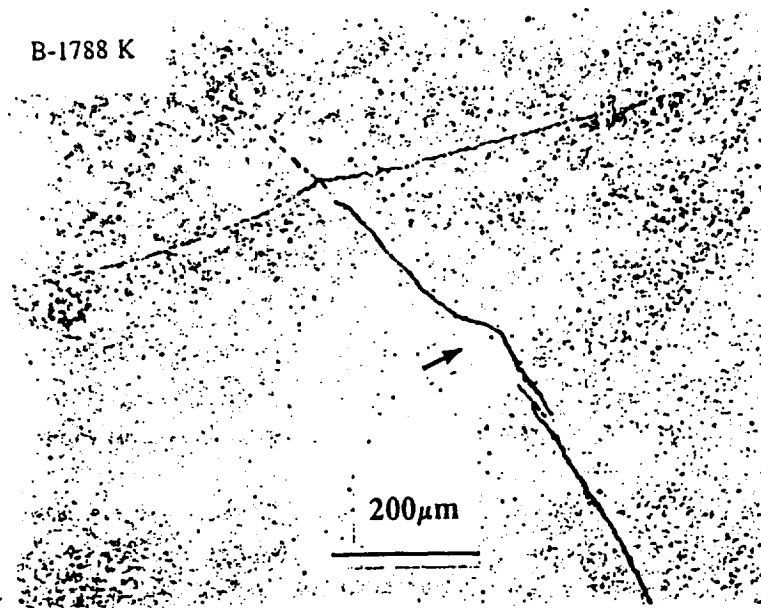


B-1743 K



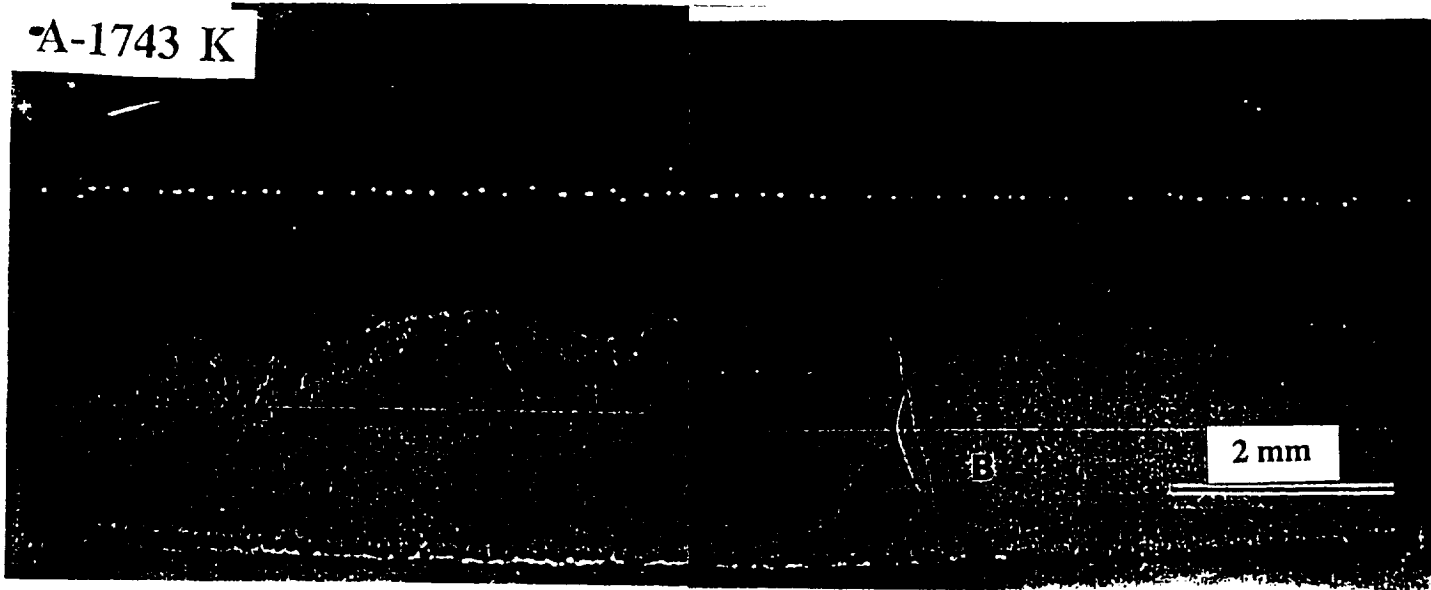
(a)

B-1788 K

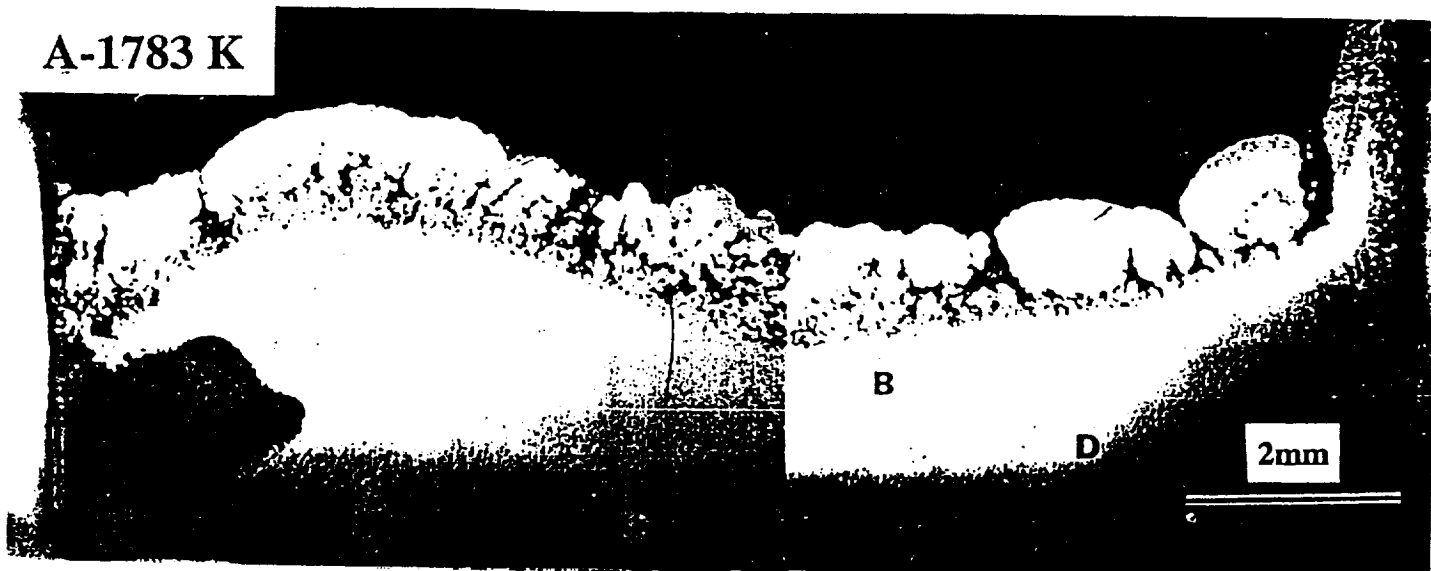


(b)

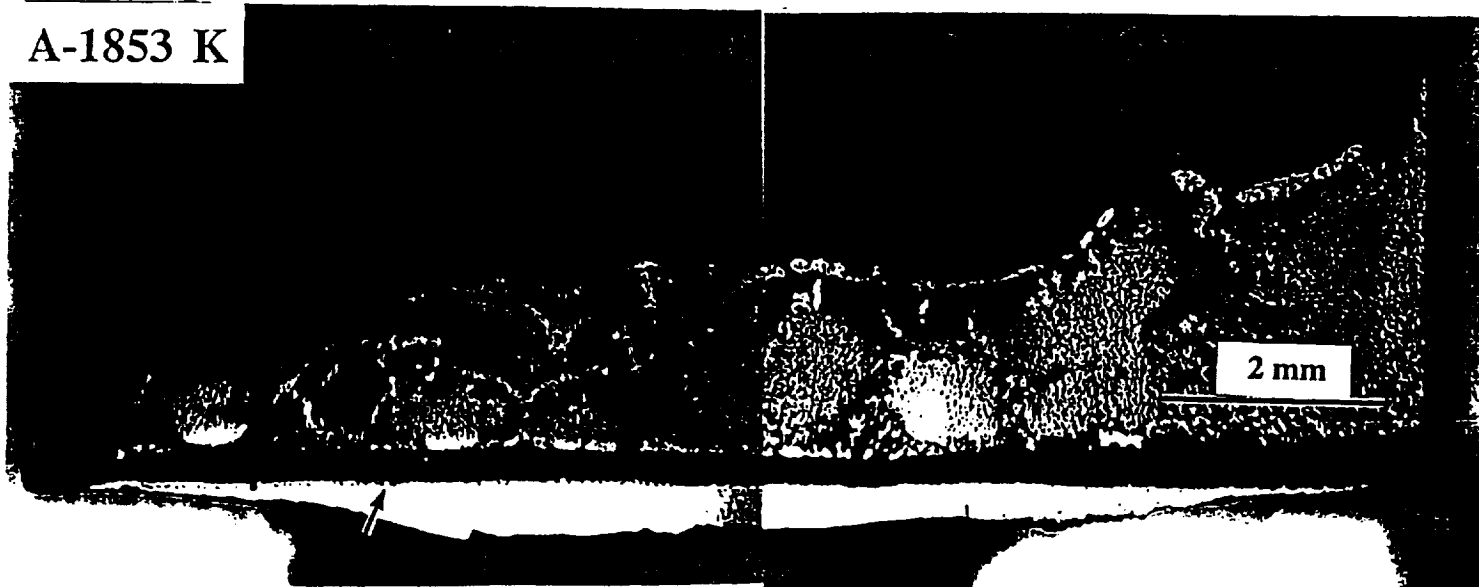
A-1743 K

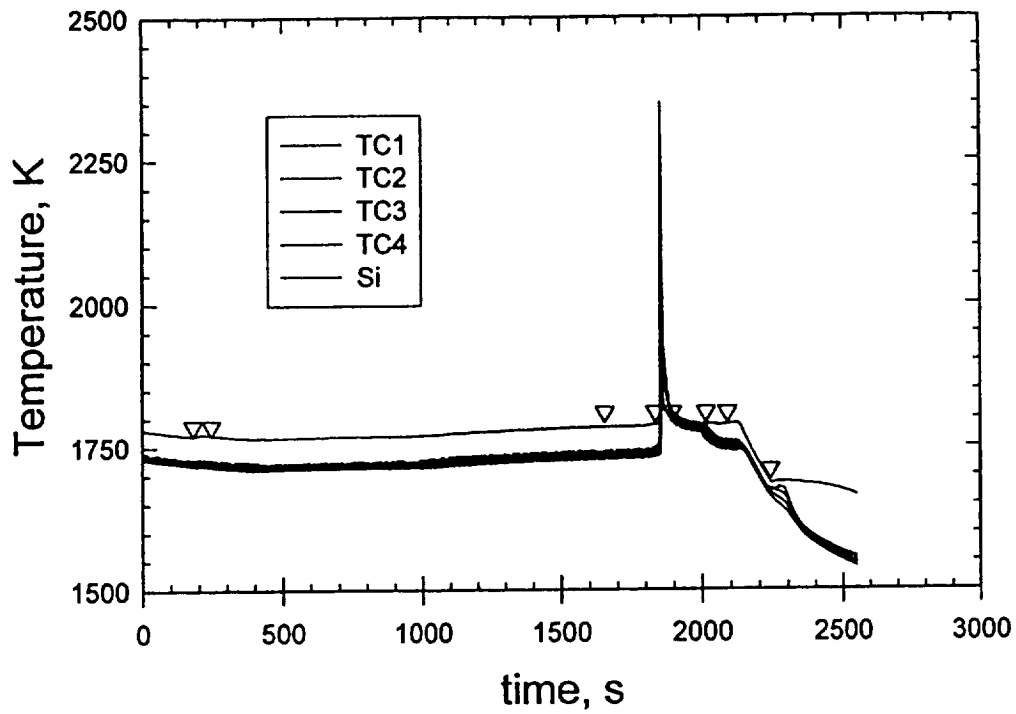


A-1783 K

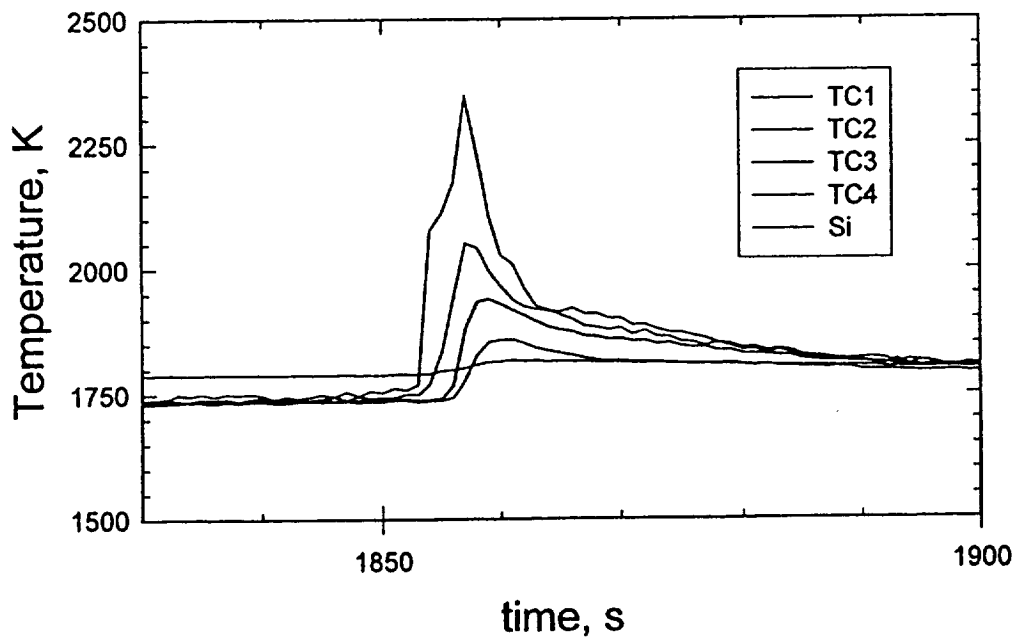


A-1853 K





(a)



(b)

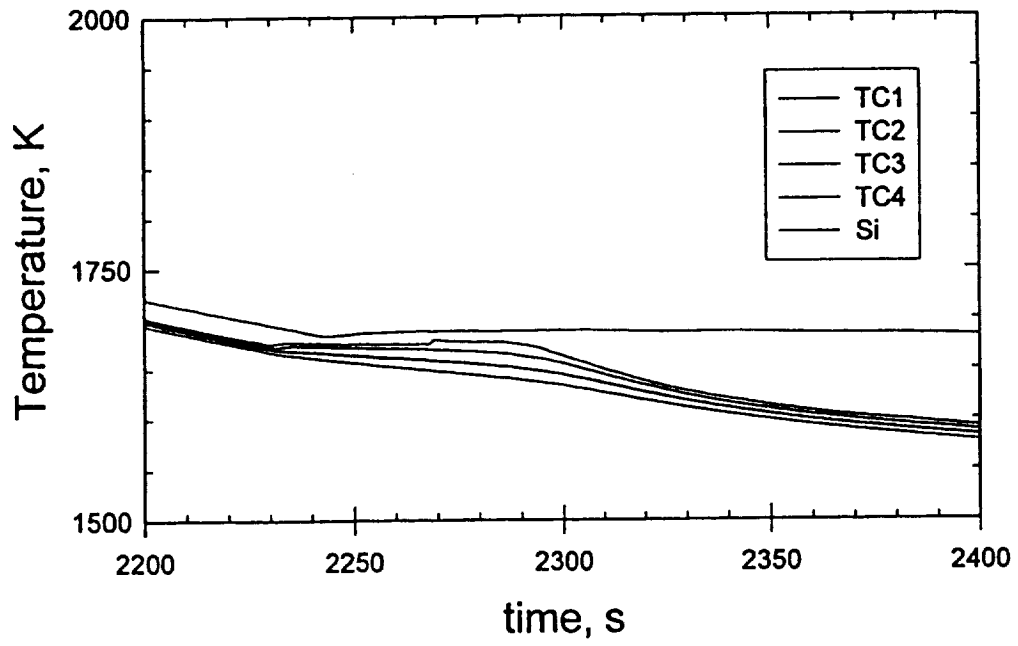


Fig 9(c)

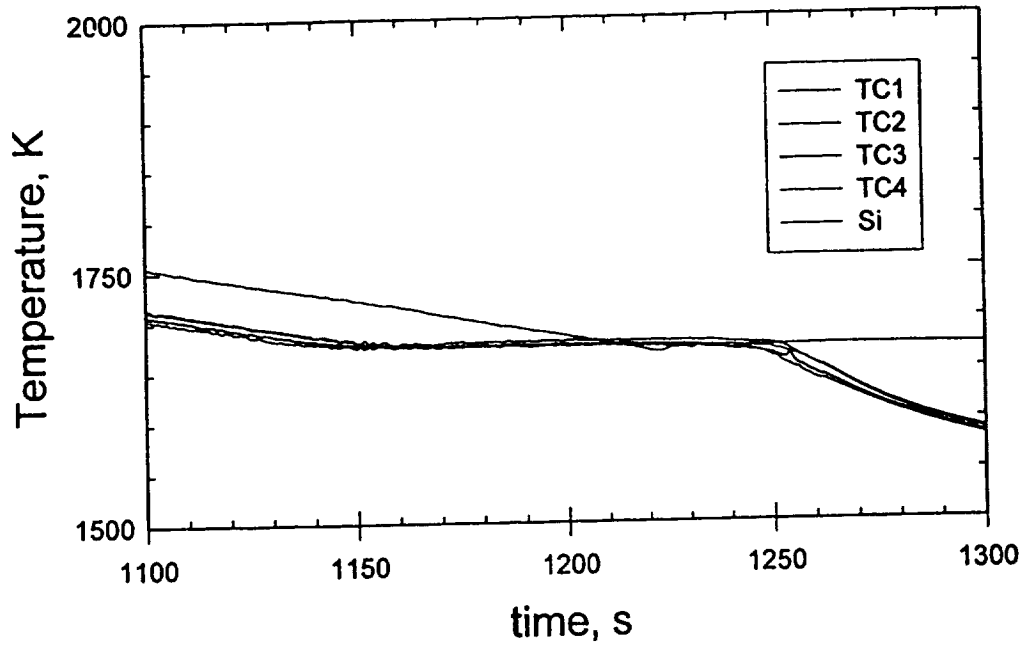


FIG 10 c)

INFLUENCE OF SPECIMEN TYPE ON THE INFILTRATION FRONT VELOCITY

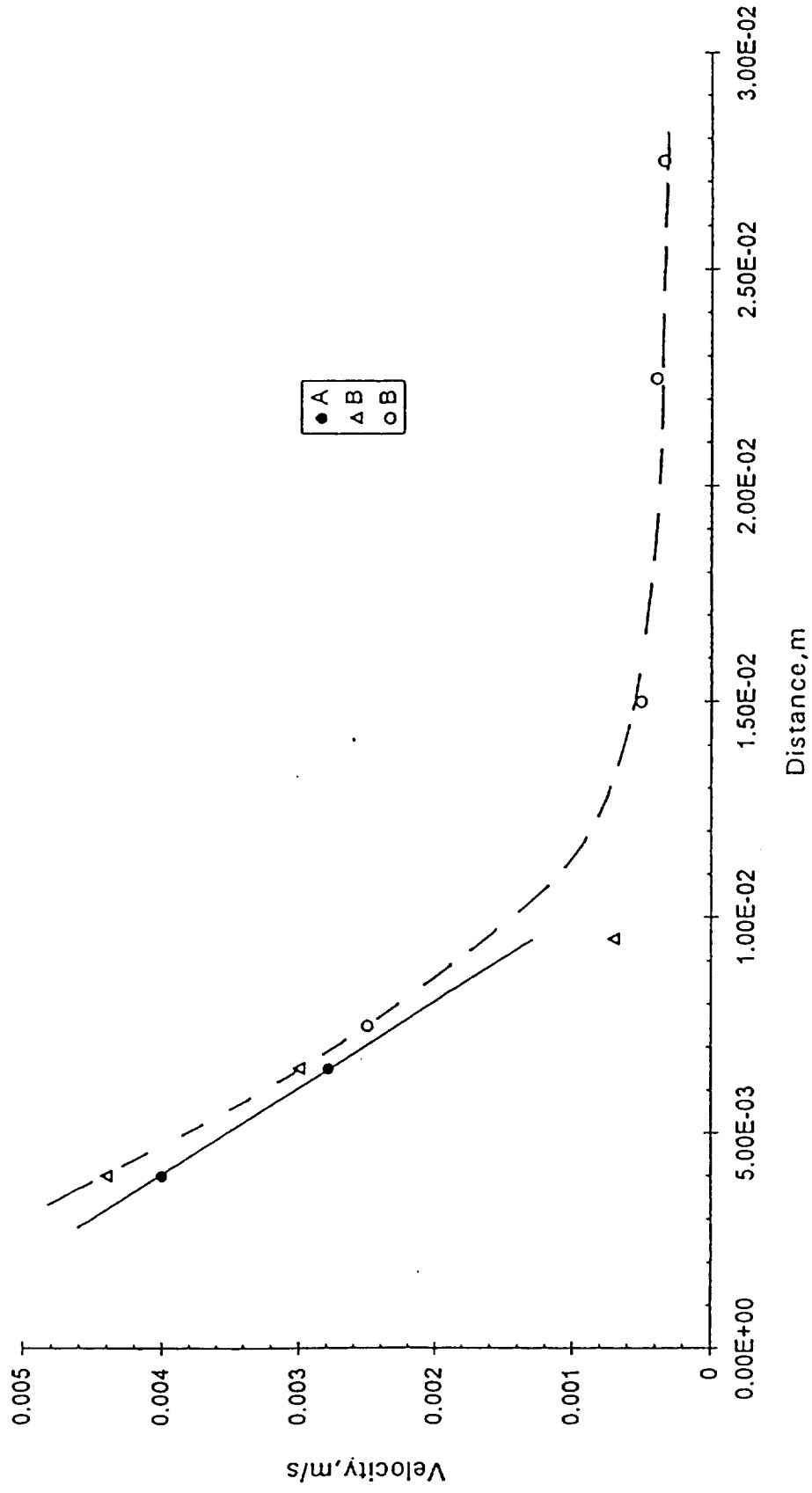


FIG 12 (a)

INFILTRATION FRONT VELOCITY AS A FUNCTION OF INFILTRATION DISTANCE

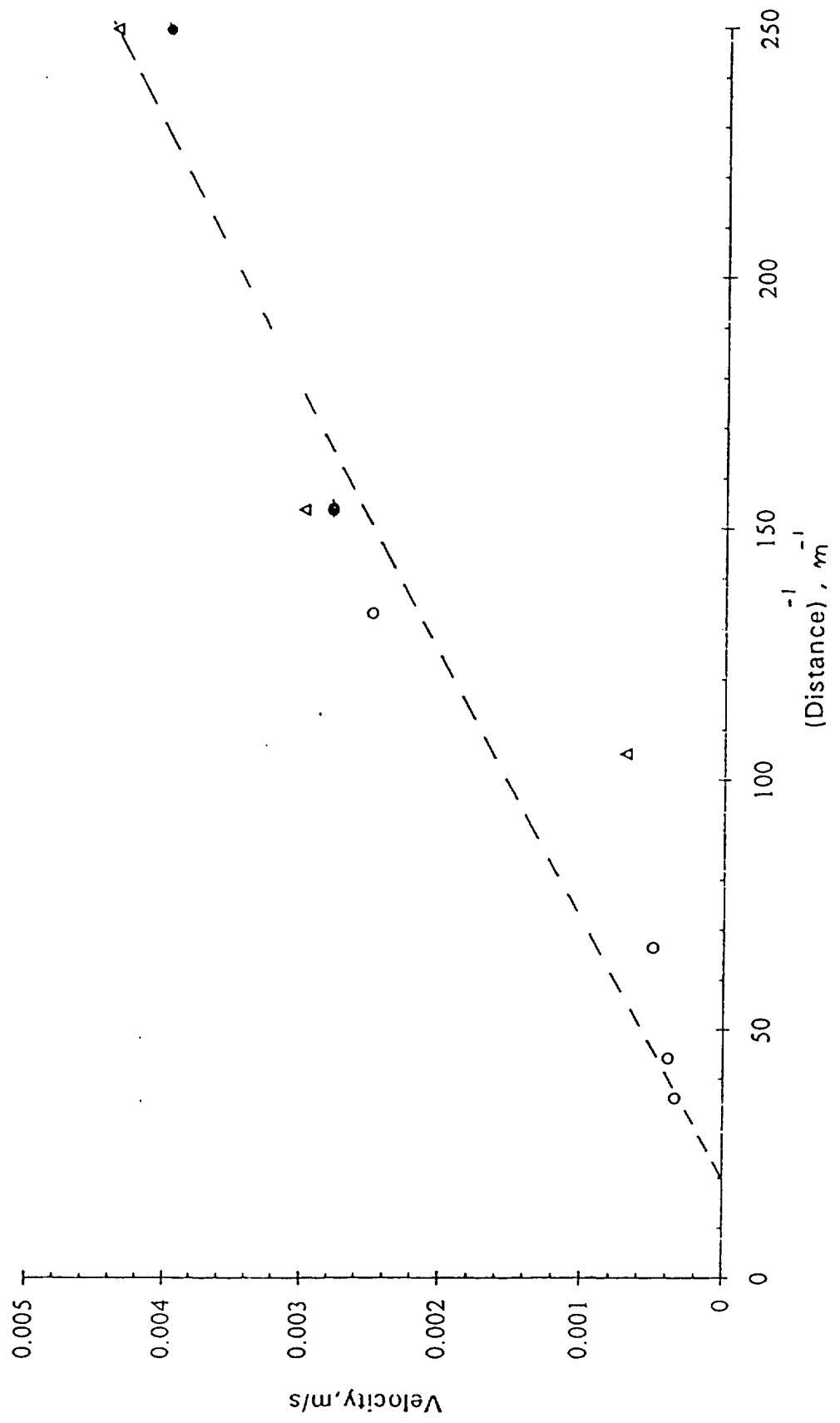


FIG. 12 (b)

THERMAL RESPONSE (Maximum temperature)

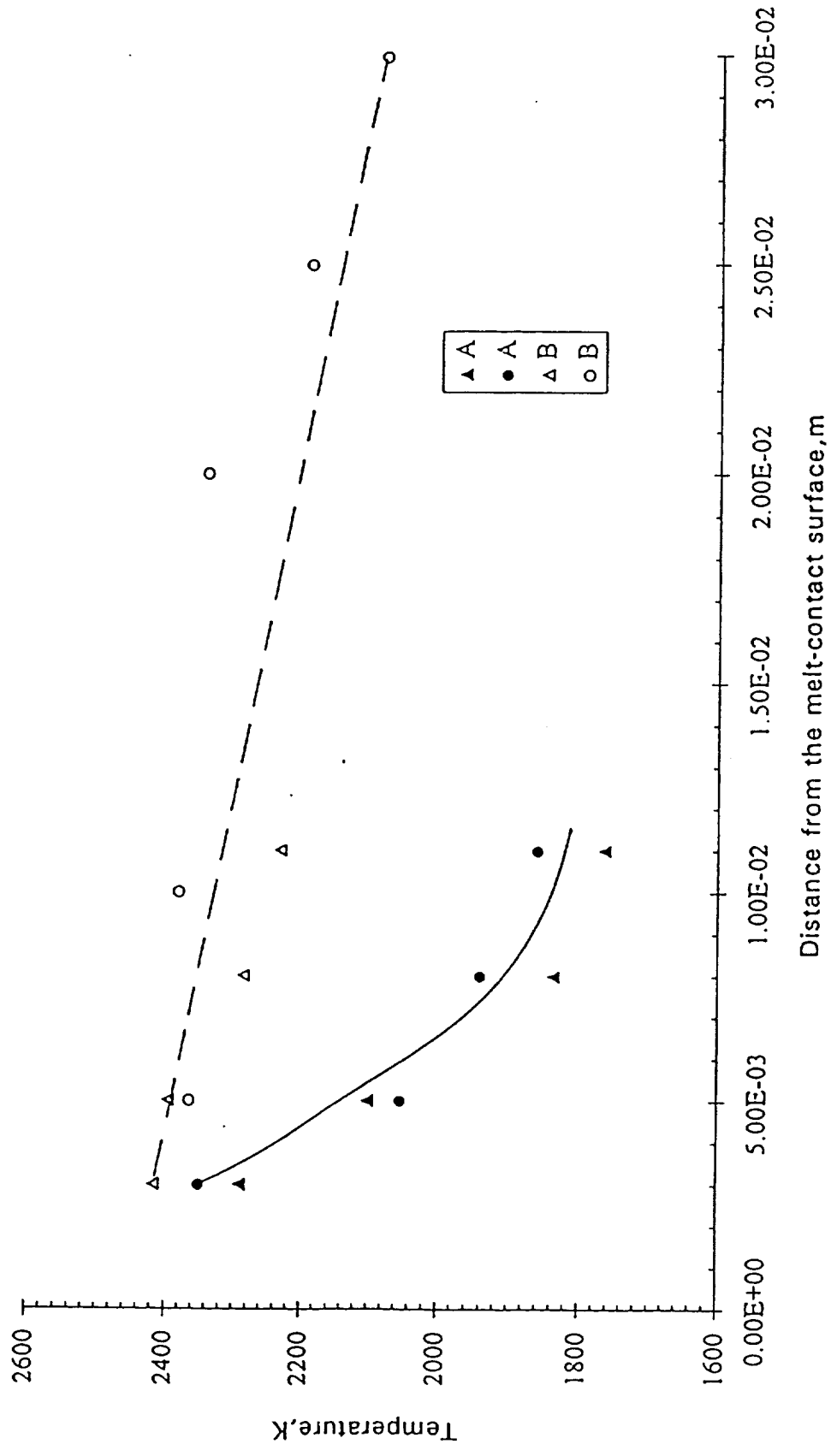


FIG 13